## *Supplementary Information*

# How the alignment of adsorbed ortho H pairs determines the onset of selective carbon nanotube etching

### Stresses in CNTs

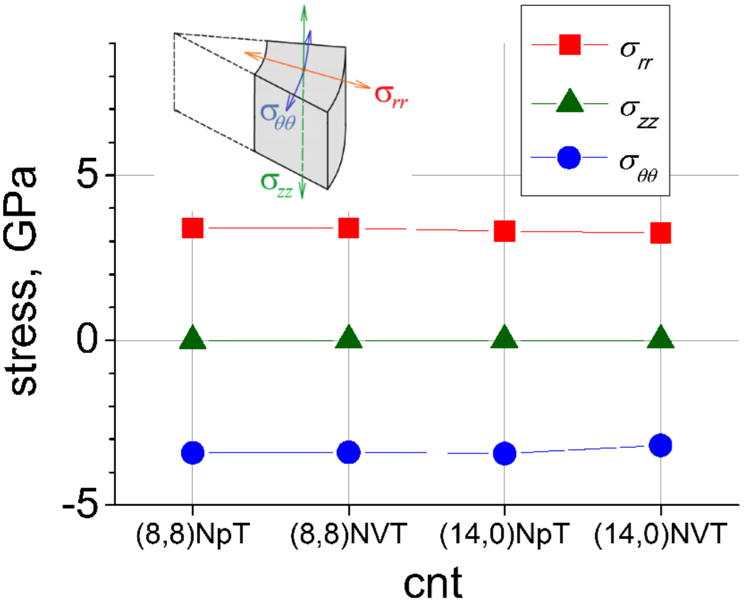

**Supplementary Figure S1** - Radial ($\sigma_{rr}$), axial ($\sigma_{zz}$) and tangential ($\sigma_{\theta\theta}$) stresses in zigzag (14,0) and armchair (8,8) carbon nanotubes prior to hydrogenation.

In figure S1, the initial radial ($\sigma_{rr}$), axial ($\sigma_{zz}$) and tangential ($\sigma_{\theta\theta}$) stresses in zigzag (14,0) and armchair (8,8) carbon nanotubes are plotted in both the canonical and the isothermal-isobaric ensemble, demonstrating that the results are similar and do not depend on the simulation boundary conditions. Here, the compressive stress is presented as a positive value, and the tensile stress as a negative value. It is clearly shown that while the radial and tangential (shear) stresses are non-zero in the nanotubes due to their curvature, while the axial stress is zero, although a periodic boundary is applied in this direction. The fact that the values for the radial stresses are equal in magnitude to the tangential stress values due to the symmetry, but opposite in sign, and that the axial stress is zero if no strain is applied, is in qualitative agreement with other MD calculation results [1].

## $H_2$ plasma irradiation system

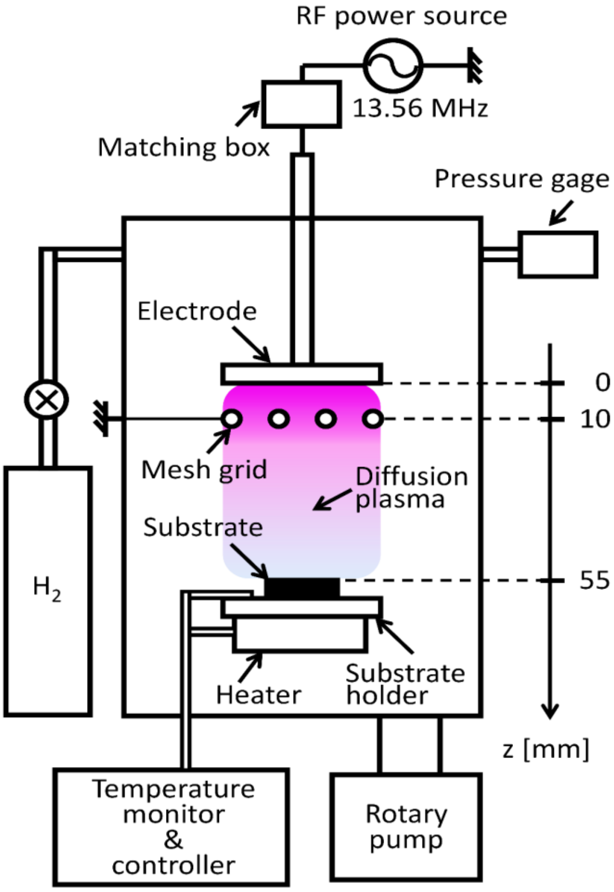

**Supplementary Figure S2** – Schematic illustration of the $H_2$ plasma irradiation system.

Hydrogen plasma irradiation was carried out by a laboratory-made diffusion plasma system (Fig. S2). The plasma was generated by a capacitively-coupled radio-frequency (RF; 13.56 MHz) discharge with planar-type electrodes at a pressure of 30 Pa. The RF power (30 W) was supplied to the upper electrode and a mesh-type electrode connected to the ground was used as the bottom electrode to promote the diffusion of plasma into the downstream region. The surface temperature of the substrate was monitored during the plasma irradiation. Since we used the plasma diffusion region, the temperature increase of the substrate during the plasma irradiation can be almost negligible (below 5 ºC).

## H-clustering effect

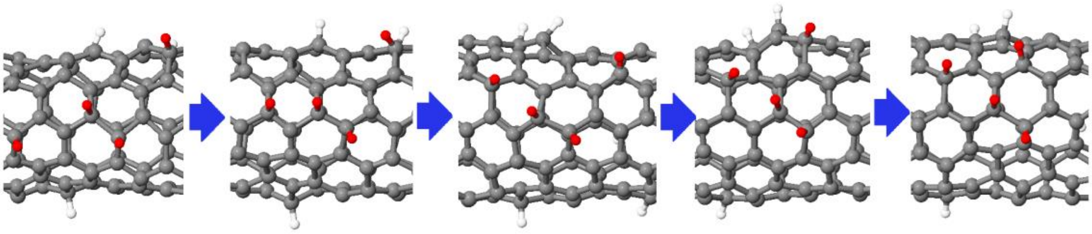

**Supplementary Figure S3 –** Coalescence of adsorbed H atoms (colored in red, for the sake of clarity) on a nanotube network during the hydrogenation process.

In Figure S3, the H coalescence (clustering) effect is demonstrated. During the hydrogenation, para, meta and ortho H pairs are initially found, but the meta pairs can eventually transform to either para or ortho pairs.

## Curvature change of CNTs for opposite sides

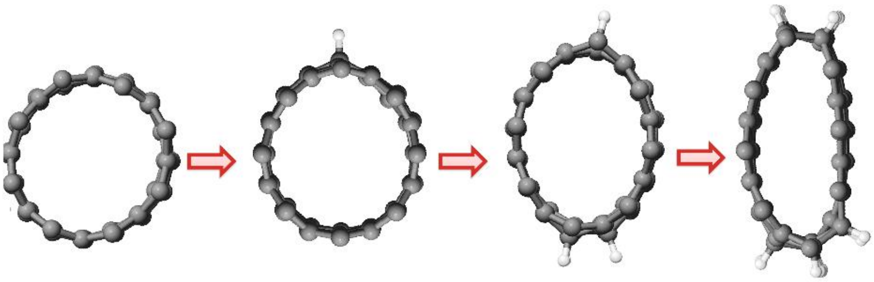

**Supplementary Figure S4 –** Curvature changing mechanism for opposite sides of the nanotube during the hydrogenation.

During the hydrogenation, incoming H atoms can adsorb or move to opposite ends of the structure due to the local curvature. Adsorbed H atoms thus also have the tendency to cluster on both sides of the elliptical nanowires as shown in Figure S4.

## H coverage of CNT surface

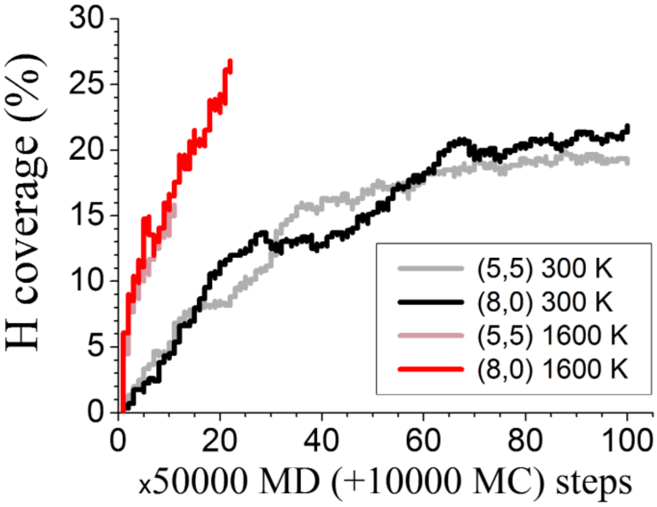

**Supplementary Figure S5 -** Evolution of H coverage on the nanotube during the hydrogenation of (5,5) and (8,0) nanotubes at low (300 K) and high (1600 K) temperatures.

In Figure S5, the evolution of the H coverage on the nanotubes at 300 K and 1600 K is shown. At low temperature, the coverage reaches about 20% before stagnating, and is similar for both the armchair (5,5) and zigzag (8,0) tubes, due to a hydrogen desorption from the nanotube either by the Langmuir–Hinshelwod recombinative desorption or the Eley–Rideal abstraction mechanisms. At high temperature, however, it can be seen that the coverage rises steeply and does not stagnate due to the easy breaking of C-C bonds in the nanotube. At about 15% coverage, the armchair (metallic) nanotube is getting etched. The zigzag (semi-conducting) nanotube, on the other hand, is not etched before a H-coverage of 27% is reached. This evolution indicates that, in agreement with most experimental observations, the metallic nanotubes are more easily etched in the simulation compared to the semi-conducting nanotubes (see also Figure S8). Also, our simulations showed that armchair nanotubes can be etched even at room temperature as well (see Figure S6). Therefore, the overall results indicate that covering about one quarter of the nanotube surface by adsorbed H atoms leads to destruction of the entire nanostructure both at low and high temperatures.

## C-C bond cleavage at room temperature

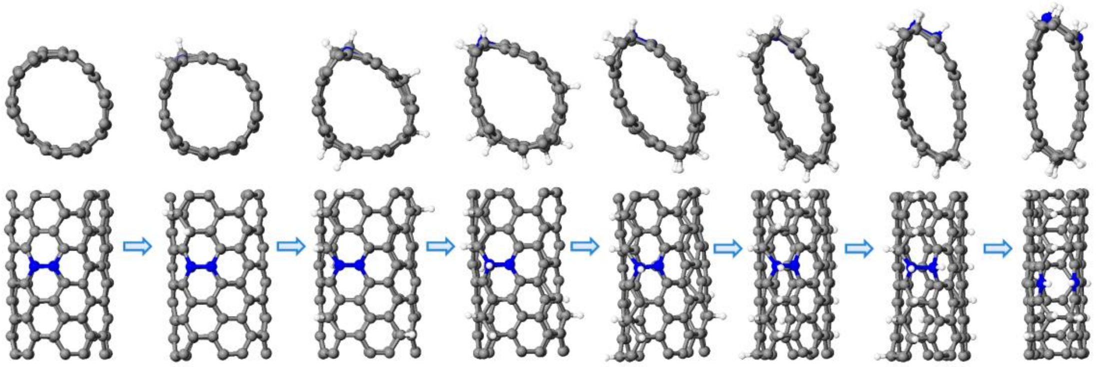

**Supplementary Figure S6 -** C-C bond breaking due to the high curvature on a (5,5) nanotube during hydrogenation at 300 K.

In figure S6, we show the evolution of H-adsorption on an armchair (5,5) nanotube at 300 K, the H-clustering and the defect formation. The first C-C bond to break is a bond perpendicular to the CNT-axis.

## First C-C bond breaking event: zigzag vs. armchair

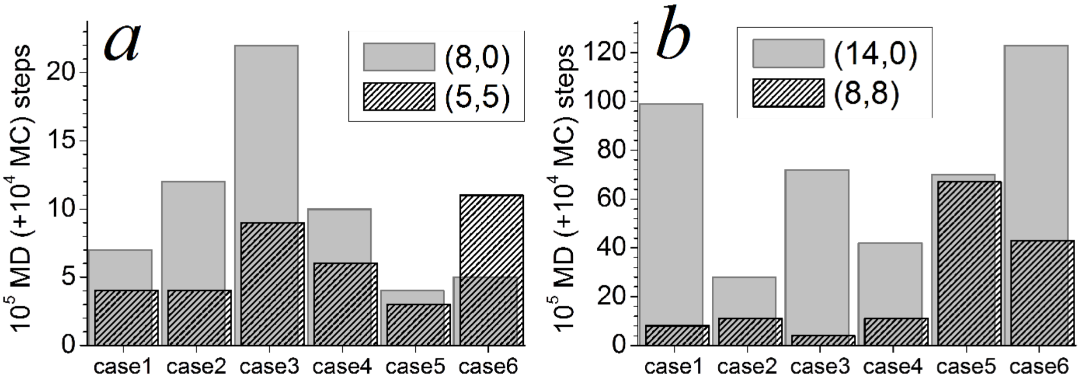

**Supplementary Figure S7 -** Number of simulation steps required for an initial C-C bond breaking event to occur in each specific case during the hydrogenation of nanotubes with diameter of about (a) 0.65 nm diameter ((8,0) and (5,5) nanotubes) and (b) 1.1 nm ((14,0) and (8,8) nanotubes).

In figure S7, we show the number of simulation steps required to observe the first C-C breaking event in armchair and zigzag nanotubes, upon equal H-exposure. It can be seen in the figure that for a small nanotube (0.65 nm diameter), in all but one case the bond breaking occurs earlier in the armchair nanotube than in the zigzag nanotube. In the case of a larger nanotube (1.1 nm), the earlier bond breaking in the armchair tube is observed in all cases. This clear difference in reactivity is observed in both the canonical and the isothermal-isobaric ensemble, demonstrating that the result does not depend on the simulation boundary conditions.

### $H_2$-plasma etching: semiconductor SWNTs vs. metallic SWNTs

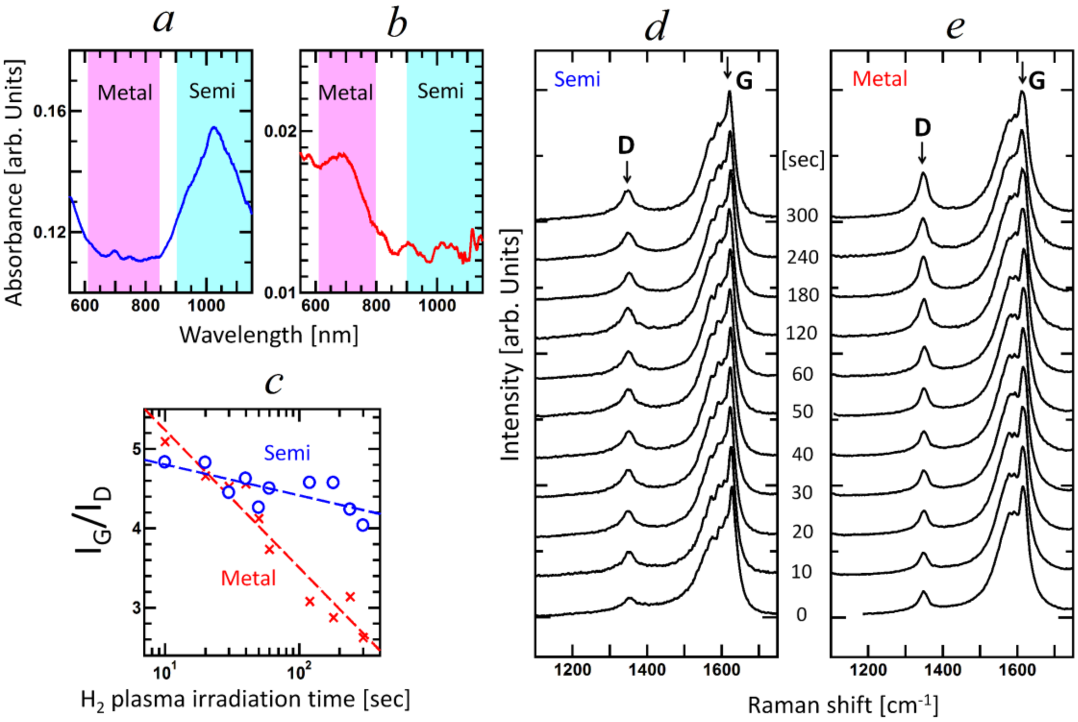

**Supplementary Figure S8** - Optical absorbance plot for (*a*) semiconductor SWNTs (99%) and (*b*) metallic SWNTs (99%) before $H_2$ plasma irradiation. (*c*) $I_G/I_D$ plot for metallic (x) and semiconductor (o) SWNTs as a function of $H_2$ plasma irradiation time. Raw Raman scattering spectra of $H_2$ plasma irradiated (*d*) semiconductor and (*e*) metallic SWNTs for different time.

The $H_2$ plasma irradiation was carried out for high purity (~99 %) semiconductor (Fig. S8a) and metallic (Fig. S8b) CNTs. The intensity ratio of the G-band to D-band ($I_G/I_D$) in Raman scattering spectra was used as a sign of the CNT quality. The time evolution of $I_G/I_D$ was measured for semiconductor and metallic CNTs. In this experiment, $H_2$ plasma irradiation (10 sec) was repeatedly performed for the same sample followed by spatial Raman mapping measurements. The $I_G/I_D$ was obtained from the same spot in the same sample, which was identified by Raman mapping measurements. Figures S8c and S8d, S8e are the plot of $I_G/I_D$ and raw Raman scattering spectra as a function of accumulated plasma irradiation time, respectively. The obvious difference can be obtained for the depletion rate of $I_G/I_D$ between metallic and semiconductor CNTs. The $I_G/I_D$ for metallic CNTs decreases much faster than that of semiconductor CNTs (Fig. S8c), indicating the metallic CNTs can be easily damaged by $H_2$ plasma.

## Supplementary references

1. Halicioglu, T. Stress calculations for carbon nanotubes. *Thin Solid Films* **312**, 11-14 (1998).